Journal of Power Sources 270 (2014) 193–200

Contents lists available at ScienceDirect

Journal of Power Sources

journal homepage: www.elsevier.com/locate/jpowsour

Thermal analysis and two-directional air flow thermal management for lithium-ion battery pack

Kuahai Yu [a, *], Xi Yang [a], Yongzhou Cheng [b], Changhao Li [b]

[a] Department of Engineering Mechanics, Henan University of Science and Technology, Luoyang 471023, PR China
[b] China Aviation Lithium-ion Battery Co., Ltd., Luoyang 471009, PR China

HIGHLIGHTS

- Numerical models are developed to predict the thermal behavior of lithium-ion battery.
- Simulation model is validated to be accurate and efficient.
- Two-directional air flow mechanism improves temperature uniformity of the battery pack.

ARTICLE INFO

Article history:
Received 15 October 2013
Received in revised form
14 July 2014
Accepted 15 July 2014
Available online 24 July 2014

Keywords:
Battery pack
Thermal management
Jet cooling
Temperature uniformity
Two-directional air flow

ABSTRACT

Thermal management is a routine but crucial strategy to ensure thermal stability and long-term durability of the lithium-ion batteries. An air-flow-integrated thermal management system is designed in the present study to dissipate heat generation and uniformize the distribution of temperature in the lithium-ion batteries. The system contains of two types of air ducts with independent intake channels and fans. One is to cool the batteries through the regular channel, and the other minimizes the heat accumulations in the middle pack of batteries through jet cooling. A three-dimensional anisotropic heat transfer model is developed to describe the thermal behavior of the lithium-ion batteries with the integration of heat generation theory, and validated through both simulations and experiments. Moreover, the simulations and experiments show that the maximum temperature can be decreased to 33.1 °C through the new thermal management system in comparison with 42.3 °C through the traditional ones, and temperature uniformity of the lithium-ion battery packs is enhanced, significantly.

1. Introduction

Lithium-ion batteries have a high-voltage, low self-discharge rate and high-energy density, and are widely employed by electric vehicles (EVs), hybrid-electric vehicles (HEVs) and avionics systems of civil aviation. The application of lithium-ion batteries is significantly restricted by safety and long-term stability demands [1,2]. The most usually technical obstacle is the temperature limitation of 0 °C–45 °C in addition to the nonuniform cell temperature in the pack [3]. Besides, overheating will deteriorate such temperature nonuniformity, thus accelerating battery degradation and reducing electric capacity, even leading to fire and explosion. Therefore, a thermal management system with enhanced stability and safety for lithium-ion batteries is highly needed.

There are two ways in the improvement of stability and safety of lithium-ion batteries. One is to look for more stable electrode materials. Although the thermal runaway usually initiates from the anode [4], the overall heat generation for the rapid temperature rise results from the chemical reaction between the cathode and electrolyte [5]. Therefore, the stable cathode structural materials draw much attentions [6–8], and it is acknowledged that $LiFePO_4$ behaves remarkable thermal stability [9,10]. An alternative way is to develop an advanced thermal management system (TMS) through passive or active cooling or heating the cells. TMS can be divided into several types based on the employment of different media such as air, liquid, phase change materials [11,12], and the media of air is the most commonly used coolant because of simple and reliable equipment requirements. Recently, accurate mathematical and numerical models describing thermal behavior of the battery have become an attractive research focus to develop effective TMS. Some models have been proposed based on transient thermal–electrochemical theory for rectilinear or spiral-wound battery

* Corresponding author. Tel.: +86 0379 64231129; fax: +86 0379 64231735.
E-mail addresses: yukuahai@hotmail.com, yukuahai@163.com (K. Yu).

http://dx.doi.org/10.1016/j.jpowsour.2014.07.086
0378-7753/

cells [13–15], and the accuracy is validated to be enough through experiments.

The conventional battery cooling system utilizes unidirectional air flow moving from the inlet to the outlet in the pack, and the convective heat transfer coefficient decreases with the air stream with the air temperature increasing. As a result, temperature of the downstream cells is usually higher than that of the upstream cells. Many efforts have tried to improve the air cooling efficiency for the batteries. For example, Xun et al. [16] found that a channel size increase could improve the cooling efficiency but led to be more unevenly distributed temperature, Fan et al. [17] also got the similar conclusions. Li et al. [18] developed a reduced-order model (two-dimensional model) to capture the dynamics of the cooling of battery modules and performed experiments to quantify the accuracy and validity. Park [19] demonstrated a parallel cooling passage design with different air flow configuration. Giuliano et al. [20] proposed a heat exchanger based on open cell aluminum foam to increase the heat transfer coefficient, and the experiments indicated that the temperature rise of the battery is restricted to just 10 °C above ambient even under 4C charge–discharge cycling. Mahamud et al. [21] developed a reciprocating air flow equipment cooling system, and the cell temperature difference oscillates within 4 °C.

Most of the literature for thermal management of lithium-ion batteries focus on the accurate mathematical modeling, the arrangement of cells and cooling efficient of conventional series/parallel channel, and there is lack of creationary of cooling mechanisms to improve the uneven cell temperature. This work explores a new air cooling mechanism to improve temperature uniformity of the lithium-ion battery pack. Three-dimensional thermal models for cells were proposed based upon the measurement of thermal and physical properties of materials. The numerical simulation results were compared directly with experimental data to quantify the accuracy and validity of the models. A new two-directional air flow cooling system is proposed, and proven in the decrease of the maximum temperature and improvement of the temperature uniformity of lithium-ion batteries.

2. Numerical computation methodology and experiments

2.1. Battery cell geometry

Fig. 1 (a) shows the 180 Ah parallel-plate prismatic lithium-ion battery (China Aviation Lithium-ion Battery CO. LTD.). The cell consists of the polymer shell, cathode and anode columns/plates, laminated core, safety vents, and gasket. The laminated core consists of dozens of aluminum film, copper film, separator, cathode and anode film, and fills up about 86% height of the battery cell, as indicated in Fig. 1(b). The rest part of the cell is filled with vacuum besides the anode and cathode current collector. The transient three-dimensional thermal computation of the battery which incorporates the heat source equations, is indeed extremely high-cost and time-consuming, especially for battery pack or box analysis. Thus, this study simplified the geometric model of the battery cell to reduce the computational cost. Some accessory structures, such as safety vent, gasket, pole bolts and nuts are ignored. The laminated core is equivalent to a solid block, and remains its anisotropic properties, which will be discussed in detail below. Fig. 1(c) illustrates the simplified geometric model.

2.2. Battery thermal model

To simplify the model without loss of generality in the thermal modeling, several assumptions are made based on the above analysis. First of all, the density of the battery materials and the electric current density distribution on the electrodes are uniform. Second, the influence of temperature on the heat capacity and conductivity of materials, and the contact resistance between current collectors and terminals are both neglected.

The governing equation for the battery cell conduction transient analysis can be written [21]

$$\rho_p C_p \frac{\partial T}{\partial t} = \nabla(\lambda_c \nabla T) + \dot{Q}_1 - \dot{Q}_2 \tag{1}$$

where, ρ_p, C_p, λ_c and T are the density, heat capacity, thermal conductivity and average temperature per unit volume, respectively. The first term on the right side of the Eq. (1) is the conductive heat transfer per unit volume. The second and third terms are the heat-generation rate and heat dissipation rate per unit volume, respectively.

Since the current density is assumed to be uniform, the heat-generation is [22]

$$\dot{Q}_1 = \dot{Q}_{joule} + \dot{Q}_{reaction} = \frac{I}{V_{cell}}\left[(U_0 - U) - T\frac{\partial U_0}{\partial T}\right] \tag{2}$$

where I, V_{cell}, U_0, and U denote the total current of the battery, the total volume of the laminated core, the open-circuit potential and

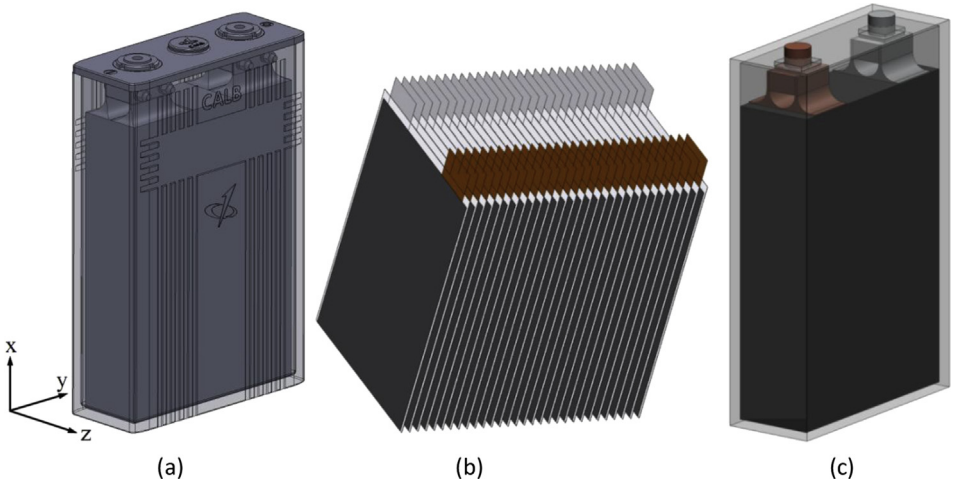

Fig. 1. 180 Ah prismatic battery cell (a) original model (b) laminated core (c) simplified unit cell.

Table 1
The internal electric resistance during 1C rate discharge.

SOC	100%	95%	90%	85%	80%	75%	70%	65%	60%	55%	50%
R_r/mΩ	0.531	0.443	0.415	0.402	0.419	0.428	0.436	0.423	0.396	0.405	0.409
SOC	45%	40%	35%	30%	25%	20%	15%	10%	5%	0%	
R_r/mΩ	0.419	0.421	0.433	0.451	0.474	0.513	0.598	0.732	0.825	0.921	

the working voltage, respectively; $\partial U_0/\partial T$ is the temperature coefficient of voltage, which can be obtained from the result of the experimental measurement. The difference of U_0 and U is expressed as IR_r. R_r is the battery internal electric resistance, which is a function of temperature and state of charge (SOC). So Eq. (2) can be described as

$$\dot{Q}_1 == \frac{I}{V_{cell}}\left[IR_r - T\frac{\partial U_0}{\partial T}\right] \tag{3}$$

The internal electric resistance R_r varies with the SOC and the temperature, the same as the temperature coefficient of voltage. We measured the two parameters during 1C rate discharge, shown as in Tables 1 and 2, respectively. The internal electric resistance decreases until 60% SOC, and then increases, especially rapidly at the end of discharge. The temperature coefficient of voltage is positive until 30% SOC. The internal electrical resistance and temperature coefficient of voltage are fitted by eighth order and sixth order polynomial as the function of SOC, respectively, and their correlation coefficients are 99.4% and 99.6%. The heat generation rate can be very conveniently calculated during transient analysis, and it has enough precision.

The heat dissipation of lithium-ion battery in this study includes the convection heat transfer (Natural convection or forced convection) and radiation heat transfer, which are the main heat exchanges between the cell surface and environments. Convective and radiative heat dissipation rate are evaluated in the following equations

$$\dot{Q}_{convection} = h\left(T_{surf} - T_{amb}\right) \tag{4}$$

$$\dot{Q}_{radiation} = \sigma\varepsilon\left(T_{surf}^4 - T_{amb}^4\right) \tag{5}$$

where h is the convection heat transfer coefficient, σ is the Stefan–Boltzmann constant and ε is the emissivity of the cell surface.

The conduction transient analysis equation can be easily calculated in the Cartesian coordinate system

$$\rho_p C_p\frac{\partial T}{\partial t} = \frac{\partial T}{\partial x}\left(\lambda_{cx}\cdot\frac{\partial T}{\partial x}\right) + \frac{\partial T}{\partial y}\left(\lambda_{cy}\cdot\frac{\partial T}{\partial y}\right) + \frac{\partial T}{\partial z}\left(\lambda_{cz}\cdot\frac{\partial T}{\partial z}\right) + \dot{Q}_1 - \dot{Q}_2 \tag{6}$$

The heat transfer and temperature rise characteristics of battery cell are greatly determined by the thermal and physical properties of the component materials with the heat source. This study measured the specific heat capacity, density and thermal conductivity of the battery shell, $LiFePO_4$ based cathode, graphite based anode, electrolyte and separator. Fig. 2 shows the test cylindrical samples of polymer shell and $LiFePO_4$ based cathode. The thermal physical properties of Aluminum and Copper are obtained from references.

The laminated core includes anode, separator, cathode, aluminum and copper films. This complicated model is reduced to a solid block to speed up calculations. The density and heat capacity is calculated based on the volume of each component [23]

$$\rho_p = \sum_{i=1}^{n}(\rho_i V_i)\Big/\left(\sum_{i=1}^{n} V_i\right)$$
$$C_p = \frac{1}{m}\sum_{i=1}^{n} C_i m_i \tag{7}$$

where ρ_p and C_p are the effective density and thermal conductivity of the laminated core, respectively. ρ_i is the density, V_i is the volume; m_i denotes the mass, m is the total mass of laminated core, i represents the part of the core structures.

Most of the laminated core is filled with liquid electrolytes, and thanks to the comparable thermal conductivity among electrolytes, separator and the electrode, their contact thermal resistance is insignificant. The arrangement of the electrode and separator along different directions can be characterized in series or in parallel (Fig. 3). The laminations in the height and width (x, y directions in Cartesian coordinate in Fig. 1(a)) are in parallel, and the thickness direction (z direction illustrated in Fig. 1(a)) is in series. When the laminations are connected in parallel, the thermal conductivity is determined by [23]:

$$\lambda_{x,y} = \frac{\sum_{i=1}^{n}\lambda_i A_i}{\sum_{i=1}^{n} A_i} \tag{8-a}$$

And when the laminations are in series, the thermal conductivity is [23]

$$\lambda_z = \frac{\sum_{i=1}^{n} L_i}{\sum_{i=1}^{n}(L_i/\lambda_i)} \tag{8-b}$$

where λ_i denotes the heat conductivity, L_i and A_i are the thickness and section area, respectively. Table 3 lists the thermal and physical properties of the component materials. The thermal conductivity of laminated core is anisotropic, and value in the z direction is much less than the other two directions.

2.3. Numerical simulation and experiments

The original battery pack contains twelve CA180 battery cells arranged into two rows, cooling plates, two fans and cooling ducts, etc., shown as in Fig. 4 (a). The outline dimensional size of the pack is 620 mm × 430 mm × 310 mm. The outwalls of the pack are all

Table 2
The coefficient of open-circuit potential and temperature during 1C rate discharge.

SOC	100%	90%	80%	70%	60%	50%	40%	30%	20%	10%	0%
$\frac{\partial U_0}{\partial T}$/VK^{-1}	0.052	0.021	0.016	0.045	0.045	0.031	0.015	−0.025	−0.063	−0.105	−0.129

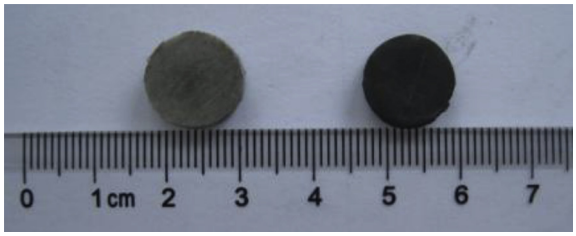

Fig. 2. Test samples of shell and anode materials.

painted aluminum plates. The cooling air sucks from the external environment through the grille inlet, and then flows to cooling battery cells. Fans are installed on the opposite side of the grille inlet.

Three-dimensional transient analysis was performed for the battery pack to predict the temperature distribution and temperature rise during 1C rate discharge and non-uniform temperature distribution issues within each battery cell. The electric current is −180 A on each cell. The heat generation rate is calculated by Equation (3), and varies with the internal electrical resistance and temperature coefficient of voltage during discharge. The fan flow rate is a function of the differential pressure, which is fitted from the experimental data. The above equations are incorporated into the FLUENT code with the User Defined Functions (UDFs) method. The calculation takes into account the transient variation of the heat generation rate, the convection heat transfer rate, the conduction heat transfer rate and the fan flow rate, simultaneously.

The fan speed is 2300 RPM, and the ambient temperature is 24 °C. The $k-\varepsilon$ two equation turbulent numerical model with a standard wall function is used for computations with the gravity effect included. The total grid is about three million. The gradients use Green-Gauss Based method. Spatial discretization uses the Second-Order Upwind finite difference method. The total solution time is 3600 s, and time step increment is 0.2 s. The computation is considered convergence when all the residuals fall below 10^{-6}.

Experiments were performed to test temperature rise of the battery cells using thermocouples. There are two rows in the pack, and six cells in each. The maximum temperature usually exists on the middle cell within the row. Temperature of the two cells was measured, and Fig. 4(b) illustrates the measurement positions. The temperature sensor probes were stuck on the center site of the batteries to monitor the surface temperature during discharge. Before the testing, the battery pack stayed in the air-conditioned environments more than three hours to keep the temperature a constant of 24 °C.

3. Two-directional air flow cooling pack design

This study proposed a new cooling device design for the battery pack, involving common air channel, vertical turning air channel and jet holes, etc. Cooling air in each channel could be supplied by one or more fans.

Table 3
Thermal and physical properties of materials. Density and heat capacity of laminated core are calculated from Formula (1), K_x, K_y are calculated from Formula (8-a), K_z is calculated from Formula (8-b).

Component	Density/ kg m^{-3}	Heat capacity/ J kg^{-1} K^{-1}	Thermal conductivity/W m^{-1} K^{-1}
Laminated core	1992.8	1363.9	$K_x = K_y = 26.1$ $K_z = 1.05$
$LiFePO_4$ based cathode	1355	1217	1.58
Graphite based anode	2217	1437.5	1.05
Separator	1008.9	1978.2	0.42
Aluminum	2702	903.1	238
Copper	8933	385	398
Shell	930	1837	0.42
Electrolyte	1124	135.8	0.63

Fig. 5 shows the schematic diagram of the two-directional air flow cooling mechanism. One uses No.1 fan to suck the air into the regular channel from one side of the pack. The cooling air, firstly, flows through the guide plate A which contains many apertures with various shapes to divert the air more uniformly and suitably. Then the air cools the battery cells, sequentially, and flows out of the grille outlet, finally.

Another air channel lies at the bottom of the pack, using NO.2 fan to suck the cooling air. The air flows through the bottom channel which is independent with the regular channel. When the air arrives at the bottom of the battery cells that need to be intensively cooled, air jets from the holes along the cells' height direction, and flows up till to meet the guide plate B, which is parallel to the cover plate and makes the jet air flow along the horizontal direction. Subsequently, the jet air confluences with the air in the regular channel, and flows out together with the air from NO.1 fan at the grille outlet, finally.

The new pack has the same dimensional sizes, material of plates and fan type with the original pack. The pack also contains twelve CA180 battery cells, and the cell thermal models were consistent with previously described. Furthermore, the computational method keeps the same with original pack simulation.

4. Results and discussion

4.1. Verification of thermal models

Fig. 6 shows the temperature rise curves of numerical simulation and experimental results. The temperature rise rate gradually decreases as discharging. The temperature difference between two test positions is about 1.2 °C at the end of the discharge. The maximum error of the temperature between the simulation and experimental results does not exceed 1 °C. It is proven that the thermal models described before have enough precision to predict the temperature rise of the battery cell.

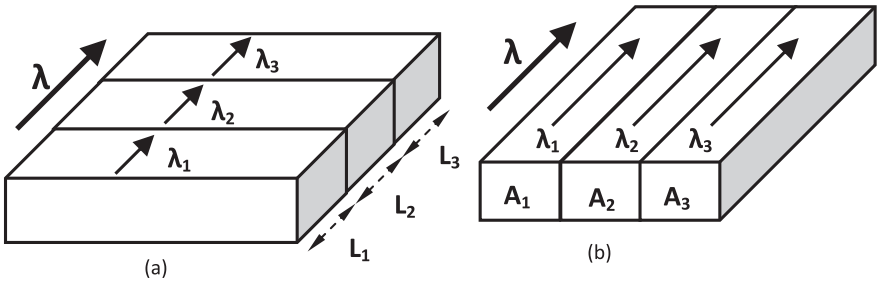

Fig. 3. Schematic diagram of effective thermal conductivity (a) in series; (b) in parallel.

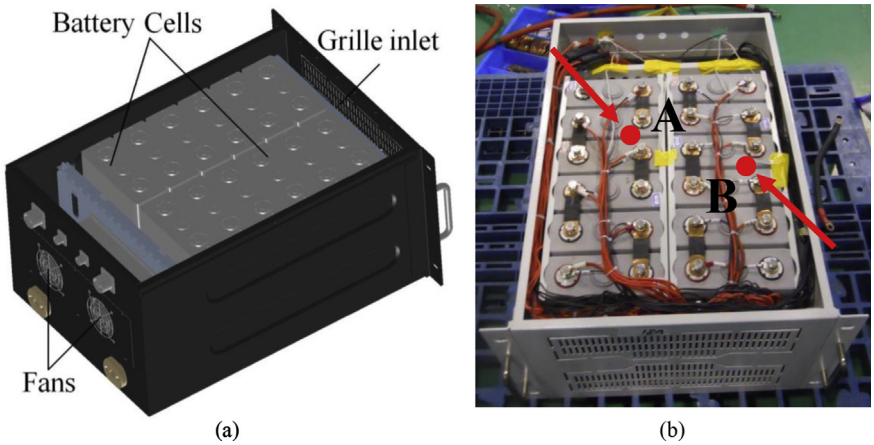

Fig. 4. CA180 battery pack and temperature measure points. (a) Geometry model; (b) experiment of temperature rise test.

Fig. 7 shows a temperature contour of the numerical results of the original pack at the end of the 1C rate discharge. The overall temperature rise of lithium-ion batteries is about 18 °C. The maximum temperature difference among cells is beyond 10 °C. The maximum temperature difference in a cell is about 8 °C. Both the temperature differences in each cell and among cells are very significantly. It greatly oversteps the principle that the maximum temperature difference in each cell should not exceed 5 °C. Thus, the battery life and performance are harmed. The maximum temperature occurs in the middle cell of the pack. The heat

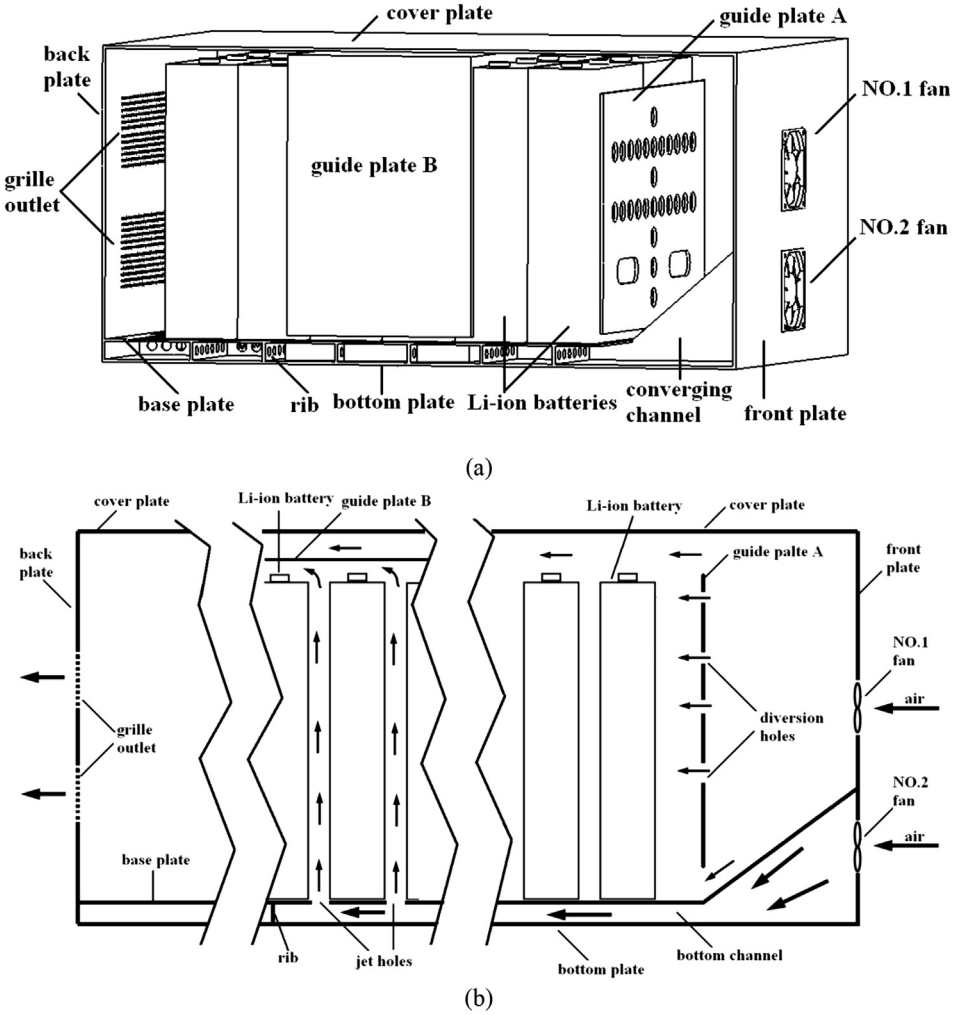

Fig. 5. Schematic of the two-directional air flow cooling pack. (a) 3D view, (b) side elevation.

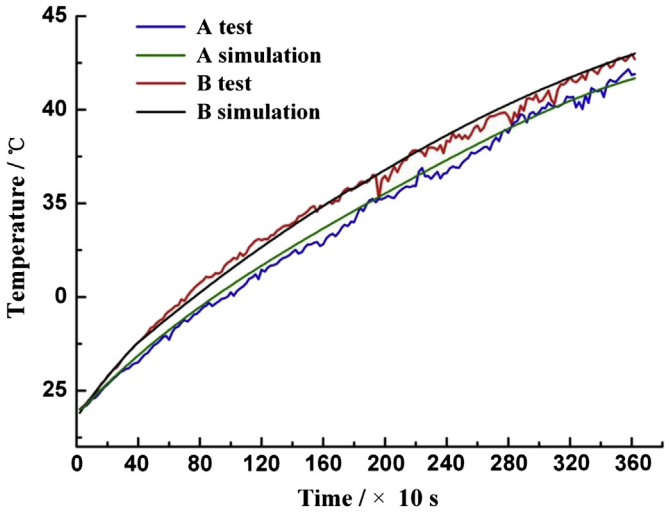

Fig. 6. Transient temperature of battery at test positions during 1C rate discharge.

accumulation happens because the air cooling is not efficient in this region. This is the common issue for conventional battery pack in series of air channels.

4.2. Results of two-directional air flow

Fig. 8 shows temperature contours of the two-directional air flow pack at the end of the 1C rate discharge. The maximum temperature of the cell is 33.1 °C, which occurs at the terminals of the cells. It indicates that the new pack can reduce the maximum temperature of the cells more than 9 °C, in comparison with the maximum temperature of 42.3 °C in the original pack. The heat accumulations in the middle cells are greatly improved, and the maximum temperature difference in each cell does not exceed 5 °C.

The streamline in the new pack is illustrated in Fig. 9. The air in the regular channel flows through the inner space of the pack uniformly, and there is no stagnation flow region. The air from the bottom fan (NO. 2), will be compressed at the converging section channel near the inlet. It is beneficial for the jet flow to cool the cells at the intermediate region.

Compared with the original pack, the new design pack has several advantageous. First, the jet hole method greatly improves

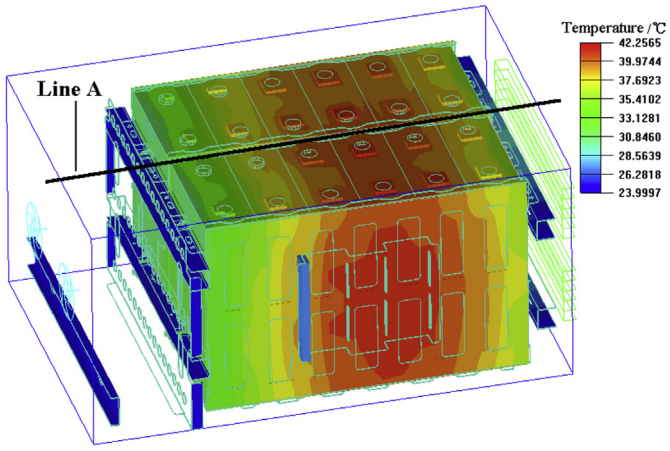

Fig. 7. Temperature contours of original lithium-ion battery pack at the end of 1C rate discharge.

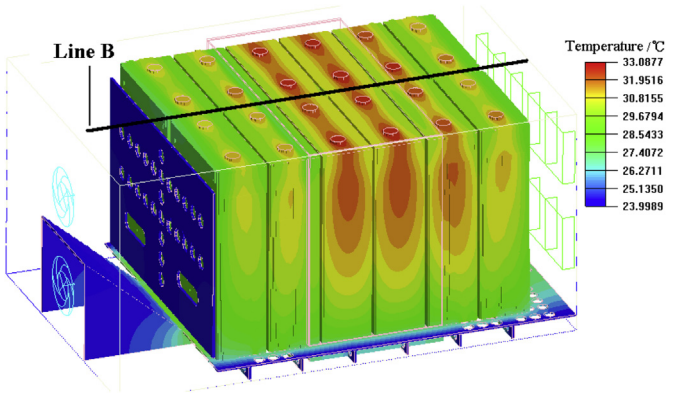

Fig. 8. Temperature contours of two-directional air flow cooling pack at the end of 1C rate discharge.

the cooling effect for the middle cells, and this is an enormous contribution in heat accumulations reduction. Second, the cooling air flows through the bottom channel of the pack will enhance the heat conduction between the base plate and the bottom of the lithium-ion battery cells, and dramatically decrease battery temperature. Third, the employment of two independent air channels eliminates the mutual interference between the two fans and improves efficiency of the fans.

4.3. Effect of air flow rate

When the volume flow rate of the air is increased, the convective heat transfer of the cells is expected to be increased. Fig. 10 shows the effect of the volume flow rate on the maximum cell temperature and the volume average temperature at the end of 1C rate discharge of the original pack and the new pack, when the ambient temperature is 24 °C. Both the maximum and averaged volume temperatures are decreased by the increase of volume flow rate, and shows a slower temperature decrease rate when the volume flow rate continues to increase. The difference between the maximum temperature and the volume average temperature of the original pack is greater than that of the new pack at the same volume flow rate. Two-directional air flow pack has a better cooling efficiency for reducing the temperature and uneven temperature distribution of the cells. Fig. 11 shows the temperature variations on the two line-profiles (Line A in Fig. 7 and line B in Fig. 8) on the middle top of the cells. The temperature distribution along the line A and line B show as parabolic and under shape, respectively. The maximum temperature occurs on the third or fourth cell along the air flow direction for both two

Fig. 9. Streamline in the two-directional air flow cooling pack.

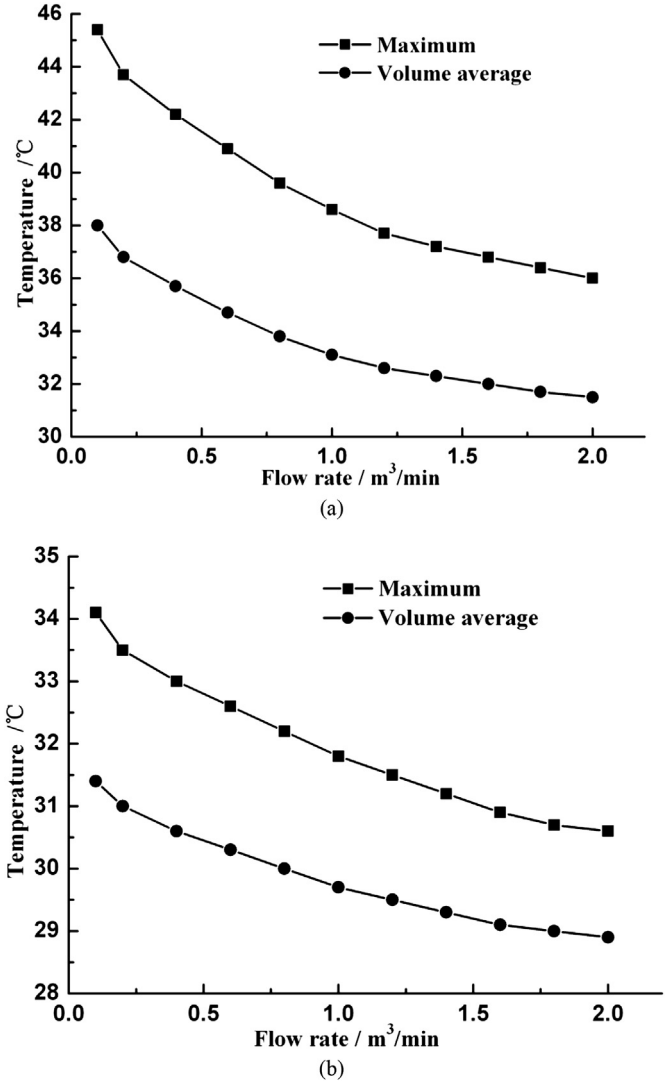

Fig. 10. Effect of the air volumetric flow rate on cell temperature: (a) original pack; (b) new pack.

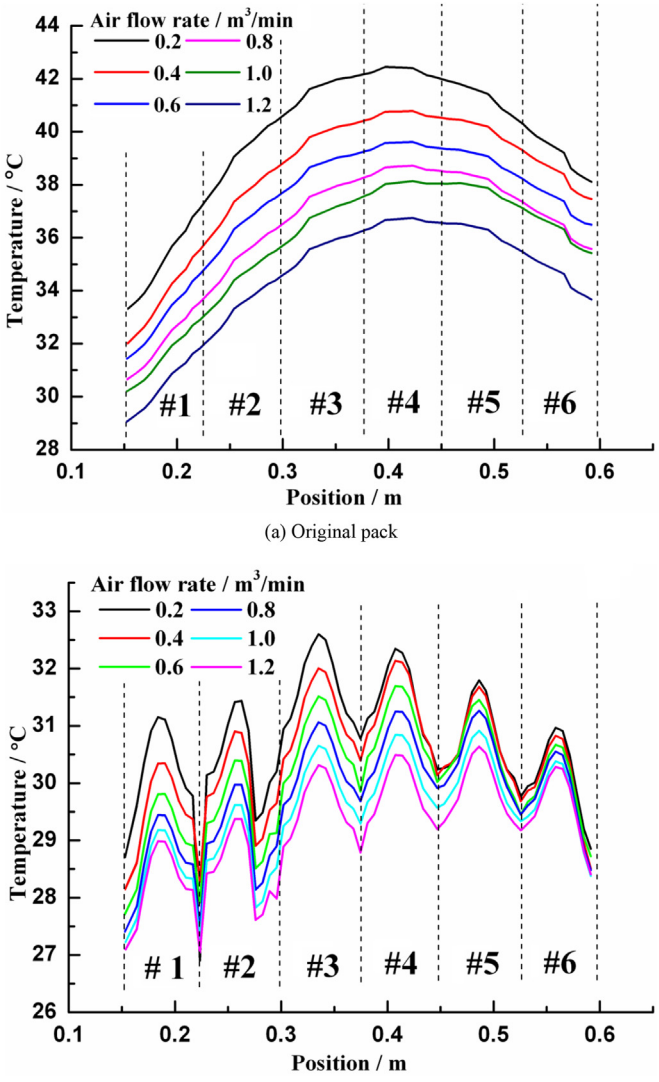

Fig. 11. Temperature variation along the air flow direction on the cells top.

packs. Fig. 11(a) shows that the heat accumulation for the middle cell can be hardly weakened by increasing the volume flow rate. The new pack has a lower temperature and more uniform temperature distribution.

The new cooling mechanism plays a higher cooling efficiency than that of the original pack. It greatly reduces the maximum temperature and improves the temperature uniformity for the lithium-ion battery pack. The contributions to this mechanism come from the proposed new design with (1) the two independent intake channels and (2) the air jet from the bottom channel.

5. Conclusions

A three-dimensional numerical model has been developed to characterize the thermal behavior of lithium-ion batteries during discharge. The model is established based on the Bernardi model and the measurement of thermal and physical properties of materials, internal resistance of battery and voltage–temperature coefficient. The accuracy of the simulation models is validated through the comparison of the temperature rise curve between experimental and computational results. The results also reveal that the temperature difference in the battery cells of the original pack is more than 10 °C, which is not positive for battery safety and life.

Two-directional air flow thermal management system is proposed to enhance the air cooling efficiency. The numerical simulation result demonstrates that the heat accumulations in the middle cells can be greatly decreased through the employment of jet cooling. At the same time, the heat conduction between the base plate and lithium-ion batteries will be enhanced by input cooling air in the bottom channel. Moreover, two independent air channels improve efficiency of the fans. The proposed method could provide a lower temperature and more uniformly temperature distribution, while keeping the pack size and the number of batteries and fans the same as the original pack, facilitating the design of high performance lithium-ion batteries with long lifetime and high reliability.

Acknowledgments

This work is supported by National Natural Science Foundation of China (51105132) and Natural Science Foundation of Henan Province (112300410166).

References

[1] Q. Wang, P. Ping, X. Zhao, G. Chu, J. Sun, C. Chen, J. Power Sources 208 (2012) 210–224.
[2] P.G. Balakrishnan, R. Ramesh, T. Prem Kumar, J. Power Sources 155 (2006) 401–414.
[3] L. Lu, X. Han, J. Li, J. Hua, M. Ouyang, J. Power Sources 226 (2013) 272–288.
[4] H.J. Bang, H. Yang, K. Amine, J. Prakash, J. Electrochem. Soc. 152 (2005) A73.
[5] J. Li, C. Daniel, D. Wood, J. Power Sources 196 (2011) 2452–2460.
[6] K. Zaghib, J. Shim, A. Guerfi, P. Charest, K.A. Striebel, Electrochem. Solid-State Lett. 8 (2005) A207.
[7] B. Scrosati, J. Garche, J. Power Sources 195 (2010) 2419–2430.
[8] G. Kucinskis, G. Bajars, J. Kleperis, J. Power Sources 240 (2013) 66–79.
[9] J.W. Fergus, J. Power Sources 195 (2010) 939–954.
[10] K. Zaghib, J. Dubé, A. Dallaire, K. Galoustov, A. Guerfi, M. Ramanathan, A. Benmayza, J. Prakash, A. Mauger, C.M. Julien, J. Power Sources 219 (2012) 36–44.
[11] Z. Rao, S. Wang, Renew. Sustain. Energy Rev. 15 (2011) 4554–4571.
[12] X. Duan, G.F. Naterer, Int. J. Heat Mass Transfer 53 (2010) 5176–5182.
[13] C. Forgeza, D.V. Doa, G. Friedricha, M. Morcretteb, C. Delacourtb, J. Power Sources 195 (2010) 2961–2968.
[14] U.S. Kima, J. Yia, C.B. Shina, T. Hanb, S. Park, J. Power Sources 196 (2011) 5115–5121.
[15] K. Somasundarama, E. Birgerssonb, A.S. Mujumdara, J. Power Sources 203 (2012) 84–96.
[16] J. Xun, R. Liu, K. Jiao, J. Power Sources 233 (2013) 47–61.
[17] L. Fan, J.M. Khodadadi, A.A. Pesaran, J. Power Sources 238 (2013) 301–312.
[18] X. Li, F. He, L. Ma, J. Power Sources 238 (2013) 395–402.
[19] H. Park, J. Power Sources 239 (2013) 30–36.
[20] M.R. Giuliano, A.K. Prasad, S.G. Advani, J. Power Sources 216 (2013) 345–352.
[21] R. Mahamud, C. Park, J. Power Sources 196 (2011) 5685–5696.
[22] S. Chacko, Y.M. Chung, J. Power Sources 213 (2012) 296–303.
[23] S.C. Chen, C.C. Wan, Y.Y. Wang, J. Power Sources 140 (2005) 111–124.